

General Disclaimer

One or more of the Following Statements may affect this Document

- This document has been reproduced from the best copy furnished by the organizational source. It is being released in the interest of making available as much information as possible.
- This document may contain data, which exceeds the sheet parameters. It was furnished in this condition by the organizational source and is the best copy available.
- This document may contain tone-on-tone or color graphs, charts and/or pictures, which have been reproduced in black and white.
- This document is paginated as submitted by the original source.
- Portions of this document are not fully legible due to the historical nature of some of the material. However, it is the best reproduction available from the original submission.

GEOS-3 Ocean Geoid Investigation

S.M. Yionoulis, A. Eisner, V.L. Pisacane, H.D. Black, L.L. Pryor

(NASA-CR-141440) GEOS-3 OCEAN GEOID
INVESTIGATION (Applied Physics Lab.) 35 p
HC A03/MF A01 CSCL 08J

N78-24776

G3/48 20843
Unclas

May 1978



National Aeronautics and
Space Administration

Wallops Flight Center

Wallops Island, Virginia 23337
AC 804 824-3411



GEOS-3 Ocean Geoid Investigation

S.M. Yionoulis, A. Eisner, V.L. Pisacane, H.D. Black, L.L. Pryor

The Johns Hopkins University
Applied Physics Laboratory
Johns Hopkins Road
Laurel, Md. 20810

Prepared Under Purchase Order No. P57,606(G)



National Aeronautics and
Space Administration

Wallops Flight Center

Wallops Island, Virginia 23337
AC 804 824-3411

CONTENTS

List of Illustrations	iv
1. Introduction	1
2. Data Preprocessor	3
3. Filter Processor	4
3.1 Martin-Graham Filter	4
3.2 Wiener Filter	5
4. Geoid Determination Processors	13
4.1 Processor I	13
4.1.1 Data Selection	13
4.1.2 Sorting	13
4.1.3 Function Evaluation	14
4.1.4 Generation of Geoidal Map	14
4.2 Processor II	14
4.2.1 Segmentation of Data into Blocks	18
4.2.2 Function Evaluation A	18
4.2.3 Function Evaluation B	19
5. Conclusions	27
Acknowledgments	28
References	29

ILLUSTRATIONS

1	Geoid Determination System Flow	2
2	Wiener Filter Geoidal Height Weights versus Time	6
3	Wiener Filter Deflection Weights versus Time	7
4	One-Second Smoothed Geoidal Height Values	8
5	Filtered Geoidal Height Values	9
6	Plot of Filtered and Smoothed Data versus Time	10
7	Filtered versus Smoothed Height Residuals	11
8	Filtered Along-Track Deflection Angles	12
9	Geoid Heights	15
10	North-South Deflection Angles	16
11	East-West Deflection Angles	17
12	Geoid Height Determined from GEOS-3 Altimeter Data Determined from Filtered Along-Track Height Data	20
13	North-South Component of the Deflections of the Vertical Determined from Filtered Along-Track Height Data	21
14	East-West Component of the Deflections of the Vertical Determined from Filtered Along-Track Height Data	22
15	Geoid Height Determined from GEOS-3 Altimeter Data Determined from Filtered Along-Track Deflection Data	24

- 16 North-South Component of the Deflections of the
Vertical Determined from Filtered Along-Track
Deflection Data 25
- 17 East-West Component of the Deflections of the
Vertical Determined from Filtered Along-Track
Deflection Data 26

1. INTRODUCTION

The primary objective of the ocean geoid investigation was to determine the fine-scale sea surface topography in the GEOS-3 calibration area using radar altimeter data. North-south and east-west components of the deflection of the vertical as well as values of the geoidal heights were estimated from an analysis of the data.

The raw data files as provided by Wallops Flight Center (Ref. 1) contained all the necessary information to compute estimates of the geoidal heights from the GEOS-3 altimeter data. Only the altimeter data taken in the short-pulse mode were used for the investigation. Three major stages of processing were used in obtaining the final results; the data flow diagram is shown in Fig. 1. The first two stages used pass processors. Each satellite pass of altimeter data over the calibration area is individually processed by these programs. Two different filter processors were investigated. The objective of the final processor was to combine all of the pass results to produce the geoidal heights and deflections of the vertical. Two different methods were also investigated in the final stage of processing.

A description of each processor is presented, as well as final results.

Ref. 1. "GEOS-C Mission Plan," TK-6340-01, Wallops Station, Wallops Island, VA.

ORIGINAL PAGE IS
OF POOR QUALITY

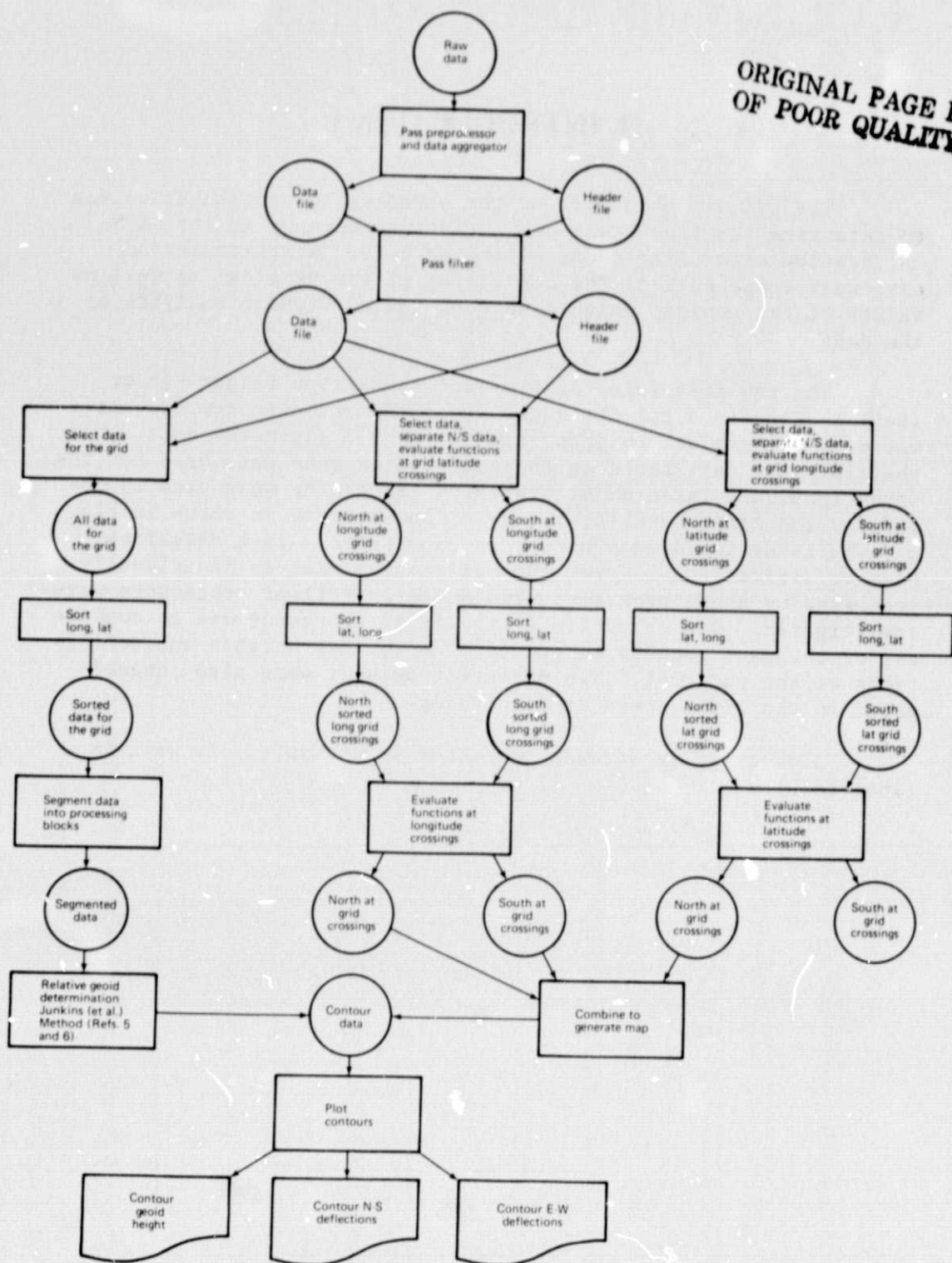


Fig. 1 Geoid Determination System Flow

2. DATA PREPROCESSOR

The major objective of the data preprocessor was to interface with the raw data as received from Wallops Flight Center and transform them into a format more easily manipulated in the subsequent stages of processing. The raw data were used to compute estimates of the geoidal heights which were then aggregated and transformed into measurements at equally spaced increments of arc distance along the satellite subtrack. A spacing of approximately 6.4 km between measurements was generated from the pass data, and data aggregation was achieved using a second-order polynomial smoother. The output of the preprocessor for each satellite pass consisted of equally spaced geoidal height measurements. The latitude, longitude, and azimuth associated with each height measurement were also saved. The azimuth defined the satellite pass direction and was used by the final data processor.

3. FILTER PROCESSOR

The objectives of the second processor were to further smooth the output from the preprocessor and to compute the along-track deflection angles from the geoidal height measurements. Two different methods were investigated:

1. A Martin-Graham low-band pass filter (Ref. 2) and
2. A filter based on the Wiener-Kolomogoroff theory (Ref. 3).

3.1 MARTIN-GRAHAM FILTER

The Martin-Graham filter was the more flexible of the two methods considered. Since it gives a choice of cut-off frequencies, filter weights could be generated that would define the highest frequency passed by the filter.

The Martin-Graham filter is characterized by the fact that its transfer function is derivable from a transfer function having a roll-off of $\cos^2 \frac{\pi(w-w_c)}{w_T - w_c}$ where w_c is the cut-off frequency, w_T the termination frequency, and w the independent variable.

Two specific low-pass Martin-Graham filters were studied for use with the GEOS altimeter data. A smoother filter was used to generate smoothed data on deflections of the vertical. In general, data having polynomial content, which is not band-limited, would be effected in a strictly band-limited filter. To circumvent this undesirable effect, both filters were developed so as to pass without distribution linear functions of the height and slopes.

Ref. 2. E. B. Anders, J. J. Johnson, A. D. Lasaine, P. W. Spikes, and J. T. Taylo, Digital Filters, NASA Report CR-136, December 1964.

Ref. 3. A. Papoulis, Probability, Random Variables and Stochastic Processes, McGraw-Hill Book Co., New York, NY, 1965.

Simulation studies were made to verify the effectiveness of the Martin-Graham filters. The selection of the cut-off and termination frequencies is of fundamental importance for use in processing the altimeter data. These determinations were to be made by studying the spectral component of local fine-scale gravity surveys. However, prior to this it was decided to abandon this approach in favor of the Wiener filter for reasons given in the following subsection.

3.2 WIENER FILTER

The method investigated used a Wiener-Kolmogoroff nonrecursive filter based on closed covariance expressions derived by Tscherning and Rapp (Ref. 4). Although not as flexible as the Martin-Graham filter, it was selected to process the data since (a) it was capable of filtering the data to the estimated noise level in the measurements ($\sigma_N \approx 24$ cm) and (b) it preserved the physical significance associated with the covariance functions used in weight computation.

Two sets of 35 weights were computed to process the data, one set for generating smoothed height data and the second for producing filtered deflection data. The weights were generated so that the filtered result was based on data symmetrically placed relative to the filtered point. Figures 2 and 3 are plots of the height and deflection weights, respectively, that were used.

Using a typical pass of preprocessed altimeter data, Figs. 4 through 8 illustrate the type of results obtained with the Wiener filter. Figure 4 is a plot of the geoidal heights before filtering. Time is used as the independent variable rather than arc distance along the satellite subtrack. (One second is equivalent to an arc distance of approximately 6.4 km.) The filtered heights are plotted in Fig. 5; both curves are shown on the same plot in Fig. 6; and the differences between the two heights are shown in Fig. 7. The filtered minus smoothed height residuals have a mean of -3.8 cm and sigma of 30 cm. Note the high-frequency structure in the residuals. The filtered along-track deflection angles are given in Fig. 8.

The filtered height and deflection data computed from each satellite pass by the filter processor are archived for use by the program used in the final stage.

Ref. 4. C. C. Tscherning and R. H. Rapp, "Closed Covariance Expressions for Gravity Anomalies, Geoid Undulations, and Deflections of the Vertical Implied by Anomaly Degree Covariance Models," Ohio State University Report No. 208, May 1974.

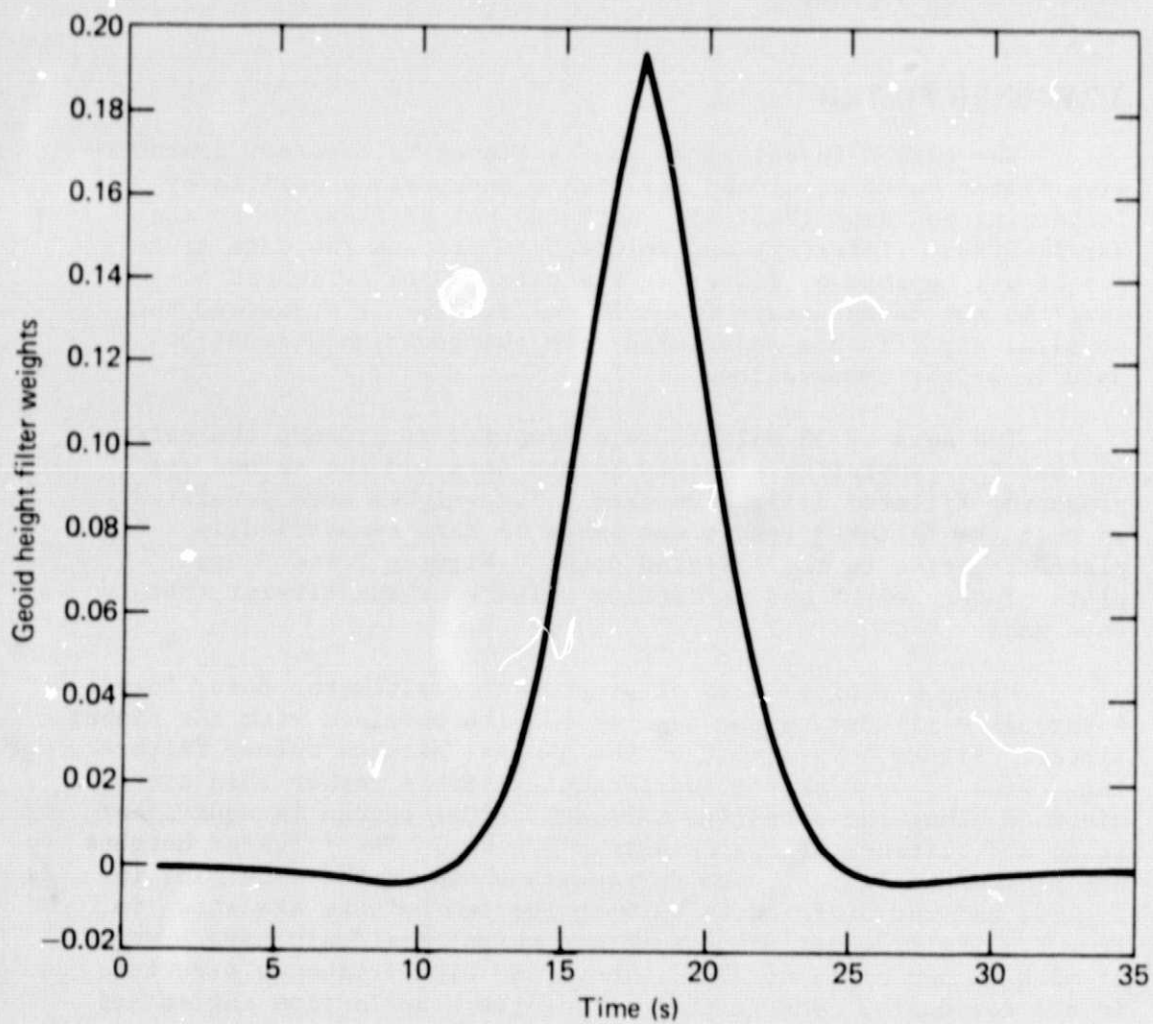


Fig. 2 Wiener Filter Geoidal Height Weights versus Time.

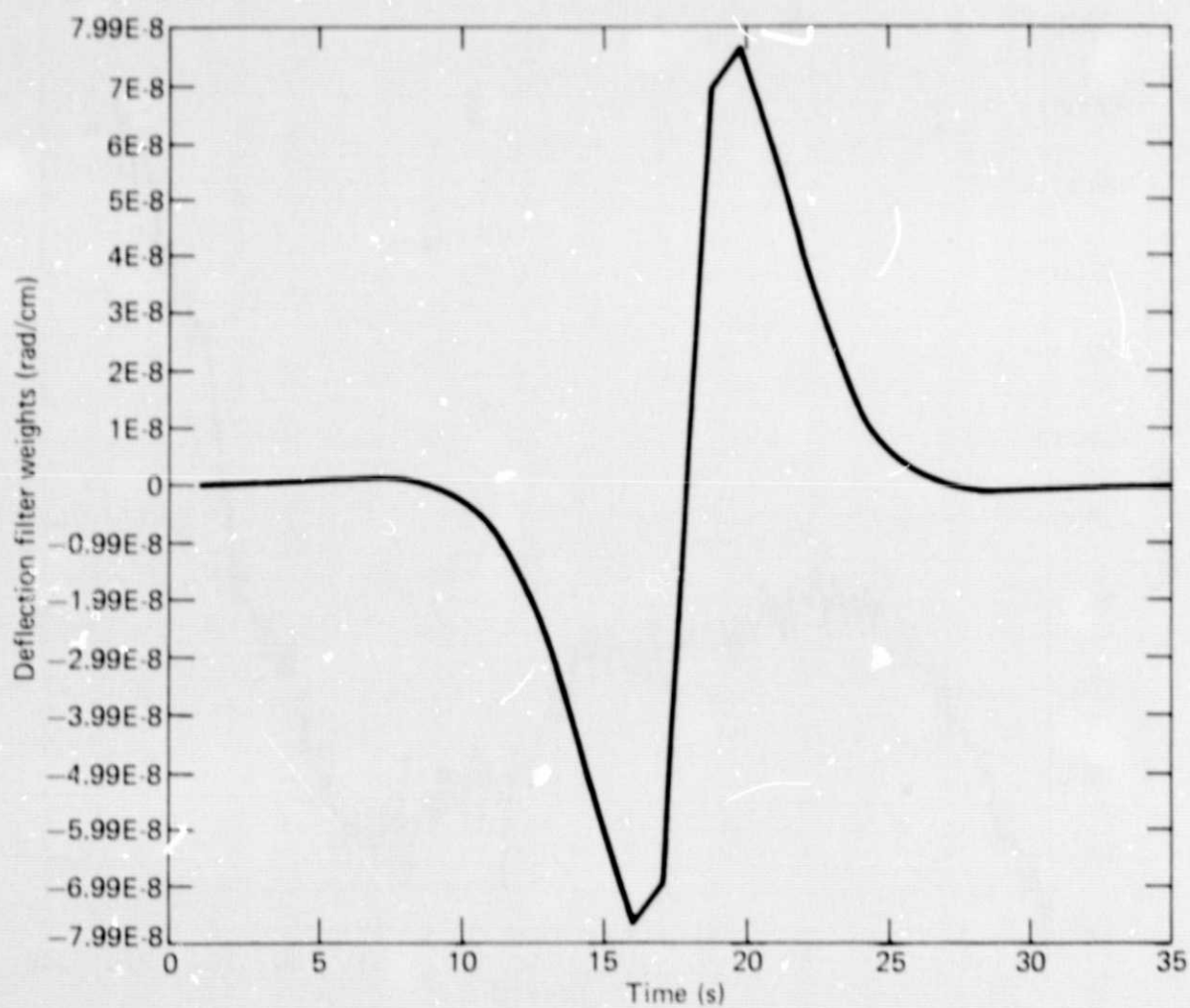


Fig. 3 Wiener Filter Deflection Weights versus Time.

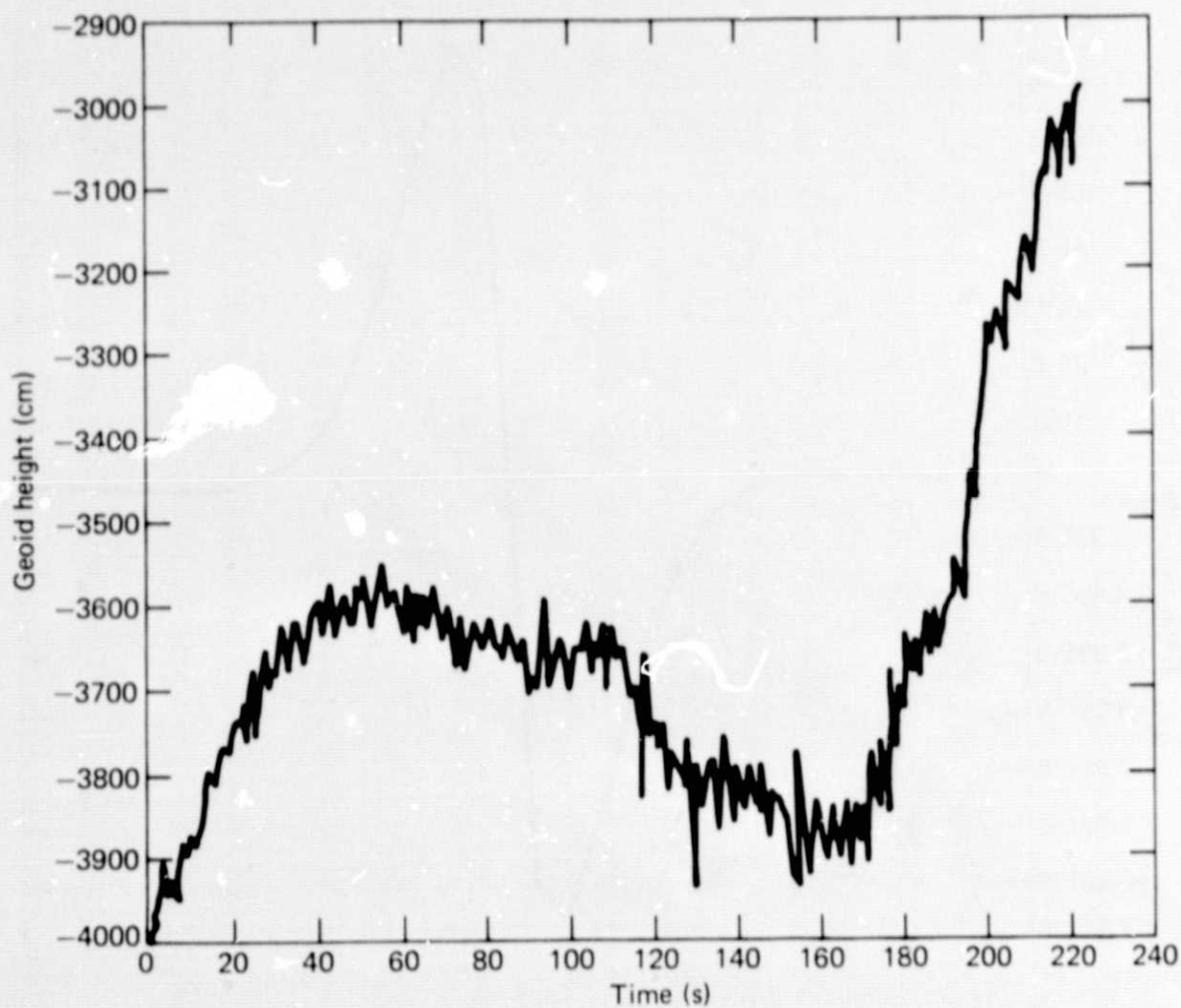


Fig. 4 One-Second Smoothed Geoidal Height Values (short pulse model).
Latitude, longitude range from (30° , 299°) to (41° , 289°).

ORIGINAL PAGE IS
OF POOR QUALITY

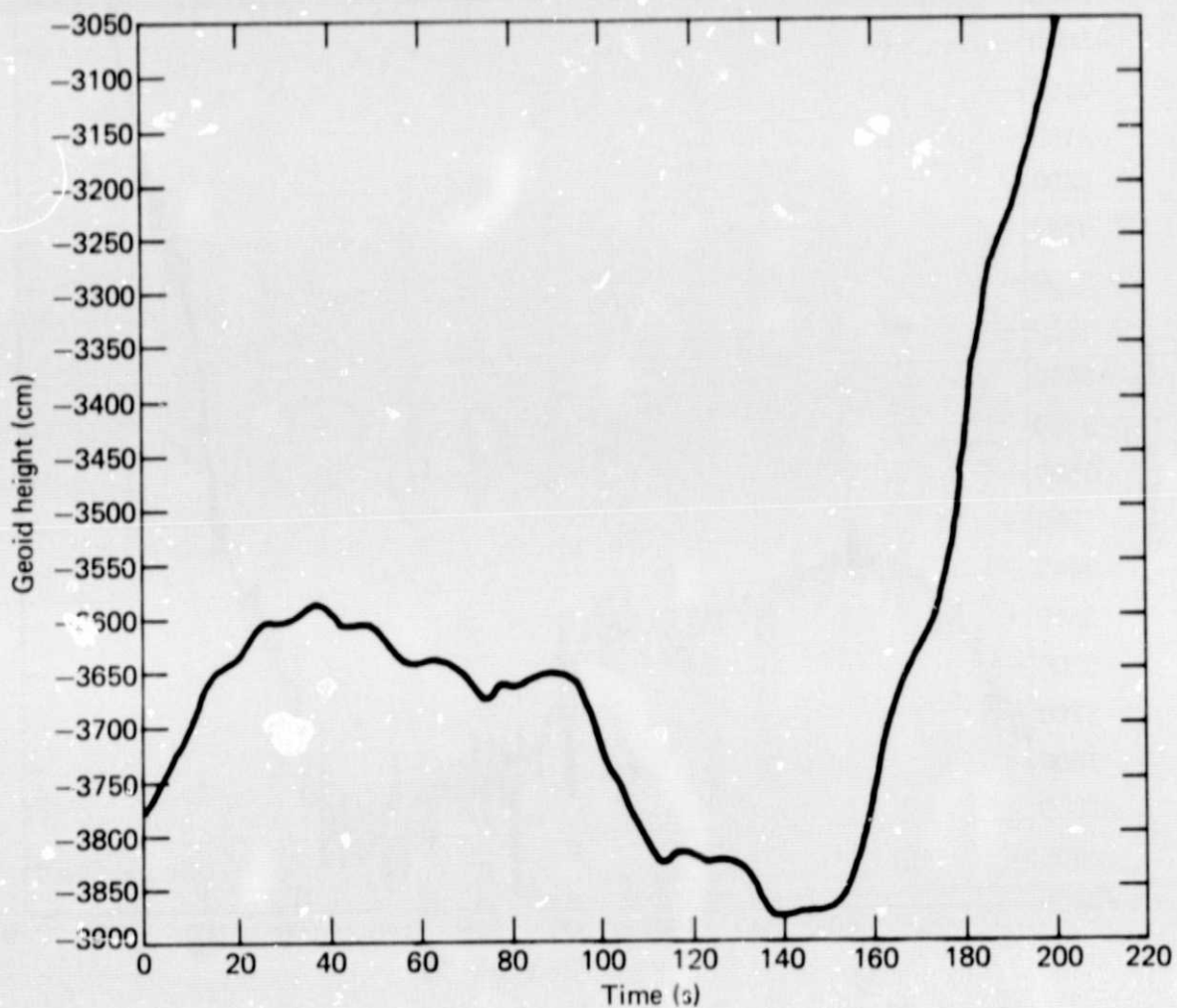


Fig. 5 Filtered Geoidal Height Values (Wiener filter, 35 weights, short pulse model). Latitude, longitude range from $(30^{\circ}, 299^{\circ})$ to $(41^{\circ}, 289^{\circ})$.

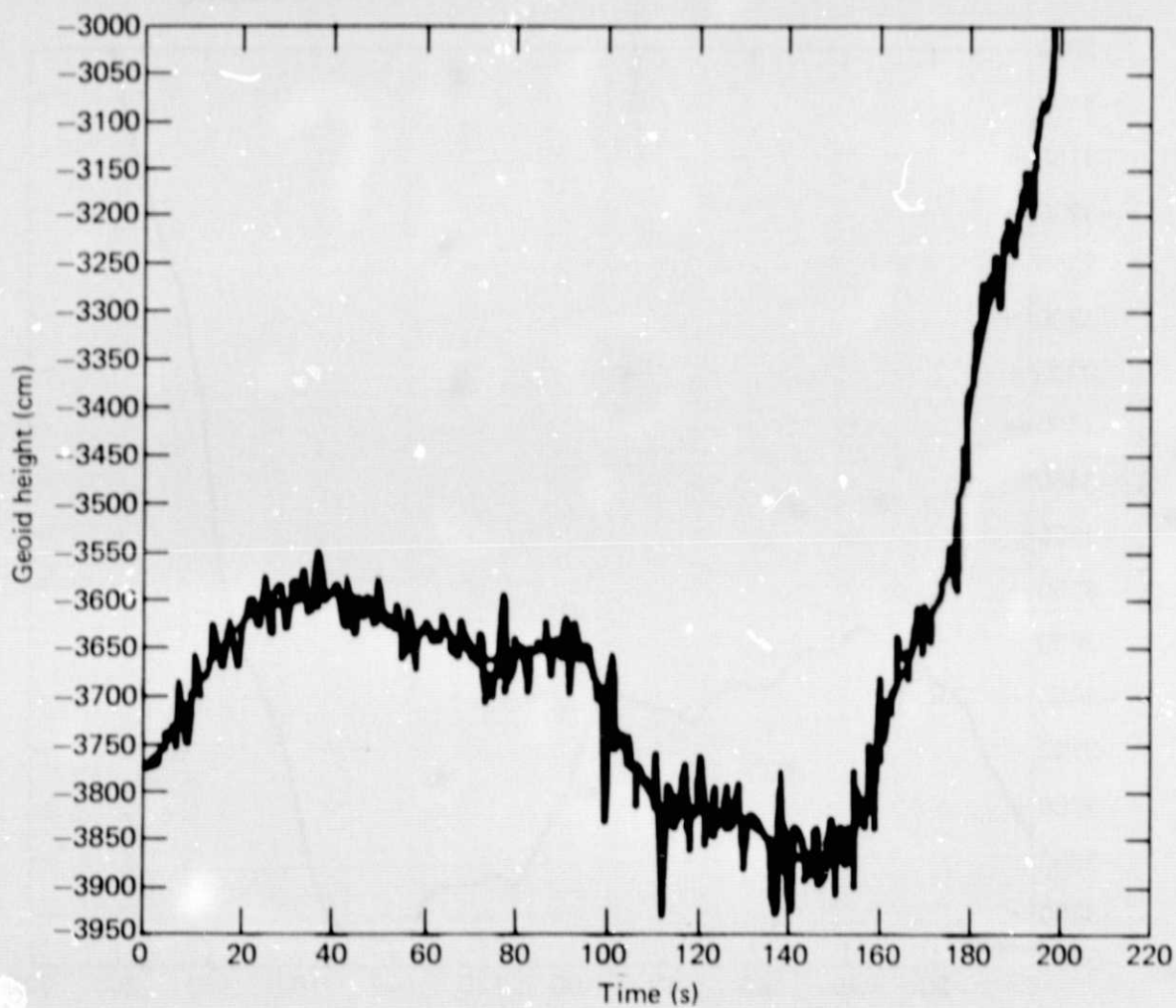


Fig. 6 Plot of Filtered and Smoothed Data versus Time

ORIGINAL PAGE IS
OF POOR QUALITY

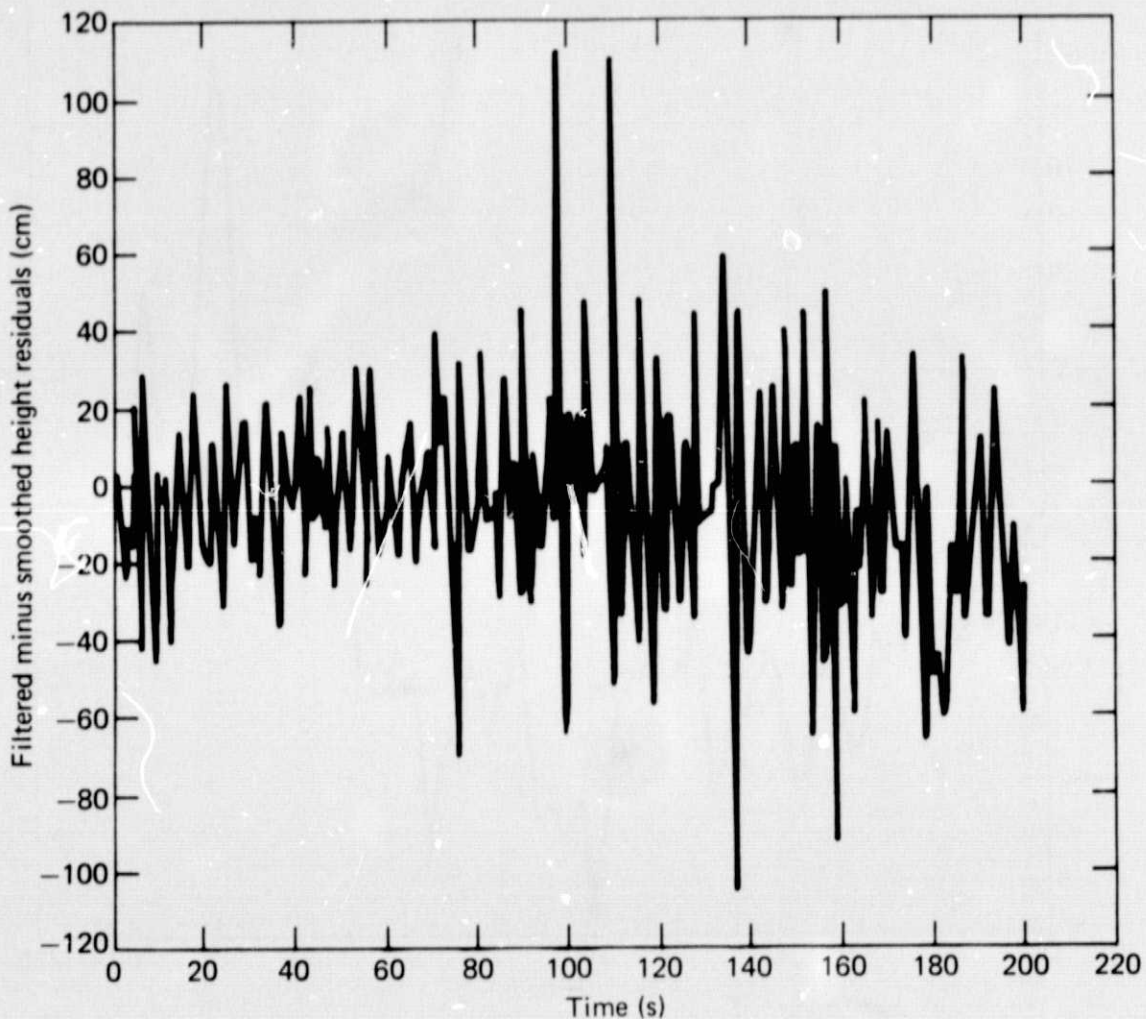


Fig. 7 Filtered Minus Smoothed Height Residuals. Mean = -3.8 cm, $\sigma = 30$ cm. Latitude, longitude range from $(30^\circ, 299^\circ)$ to $(41^\circ, 289^\circ)$.

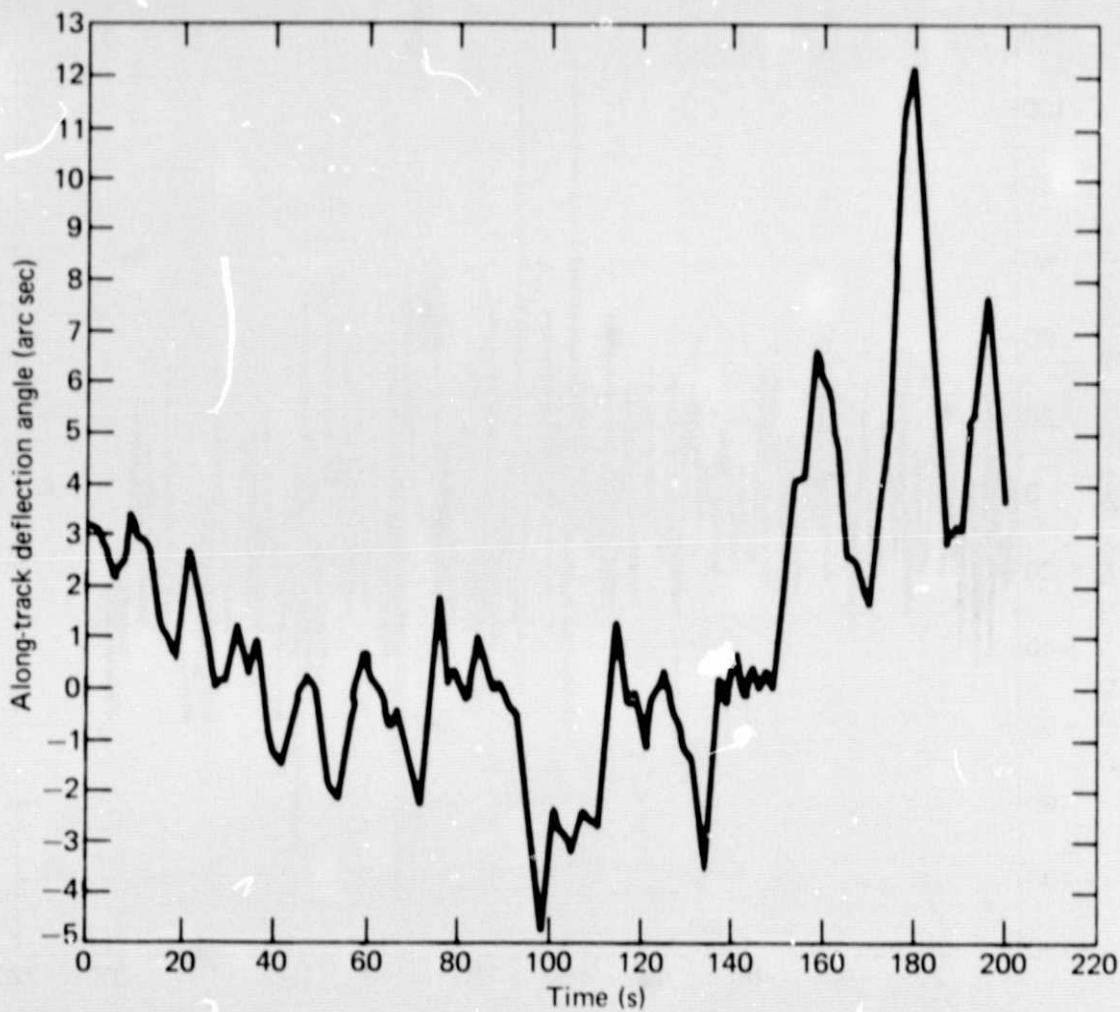


Fig. 8 Filtered Along-Track Deflection Angles (Wiener filter, 35 weights, short pulse mode). Latitude, longitude range from (30° , 299°) to (41° , 289°).

4. GEOID DETERMINATION PROCESSORS

The objective of the final stage of processing was to combine all of the pass results to produce geoidal heights and both components of the deflection of the vertical. The data were processed using two different methods. Brief descriptions of each and the results obtained are given below.

4.1 PROCESSOR I

It was intended that the first processor be made as simple as possible, yet provide reasonable value checks for the subsequent processors. Thus the following approach was implemented.

4.1.1 Data Selection

Filtered passes outside the calibration grid were eliminated. Within each pass only data confined to the calibration grid were kept. Following the selection process, the pass boundaries were ignored. Processor I had two additional functions at this stage:

1. To separate south- and north-going data and
2. To evaluate the functions at latitude or longitude grid intersections.

The functions evaluated were geoidal height, deflection angle, and either latitude or longitude. The "evaluation" was a simple averaging of all data in the vicinity ($\pm 1^\circ$) of each latitude or longitude grid intersection. Noisy data were eliminated using 3-sigma testing.

4.1.2 Sorting

A standard sorting program was used that took the data and sorted them into latitude, longitude or longitude, latitude order. With Processor I, the data have already been evaluated at either latitude or longitude grid intersections. However, for Processor II, all the data must be sorted.

4.1.3 Function Evaluation

The next module in Processor I operated on the sorted data to evaluate the functions at either latitude or longitude grid intersections. The evaluation was a simple averaging of all data in the vicinity ($\pm 1^\circ$) of each latitude or longitude grid intersection. (If data are at latitude grid intersection, then the averaging is for longitude grid crossing and vice versa). The output of this program is a table (file) of geoidal heights and deflections at grid intersections.

4.1.4 Generation of Geoidal Map

The final step in Processor I is to combine the four tables (files) and to generate a map (table) of geoidal heights and east-west and north-south deflections of the vertical. The north-south pairs are averaged and then combined to generate the east-west and north-south deflection angles. The geoidal height table is produced by averaging the north and south geoidal heights. The results obtained with this processor are shown in Figs. 9 through 11.

4.2 PROCESSOR II

The second method incorporates a weighting function approach for the modeling of irregular surfaces developed by Junkins et al. (Refs. 5 and 6). This method has many features desirable in processing large quantities of data. It allows the user to partition the data into a sequence of overlapping subsets, each of which is processed separately. A separate model is used in fitting each subset of data that is applicable only for that subset, thus requiring overall a less sophisticated model. By the use of weighting functions, nth-order continuity across boundaries of the subsets can be enforced. A complete explanation of the method is given in Refs. 5 and 6.

Ref. 5. J. L. Junkins, G. W. Miller, and J. R. Jancaitis, "A Weighting Function Approach to Modeling of Irregular Surfaces," J. Geophys. Res., Vol. 78, No. 11, 10 Apr 1973.

Ref. 6. J. R. Jancaitis and J. L. Junkins, "Modeling in n Dimensions Using a Weighting Function Approach," J. Geophys. Res., Vol. 79, No. 23, 10 Aug 1974.

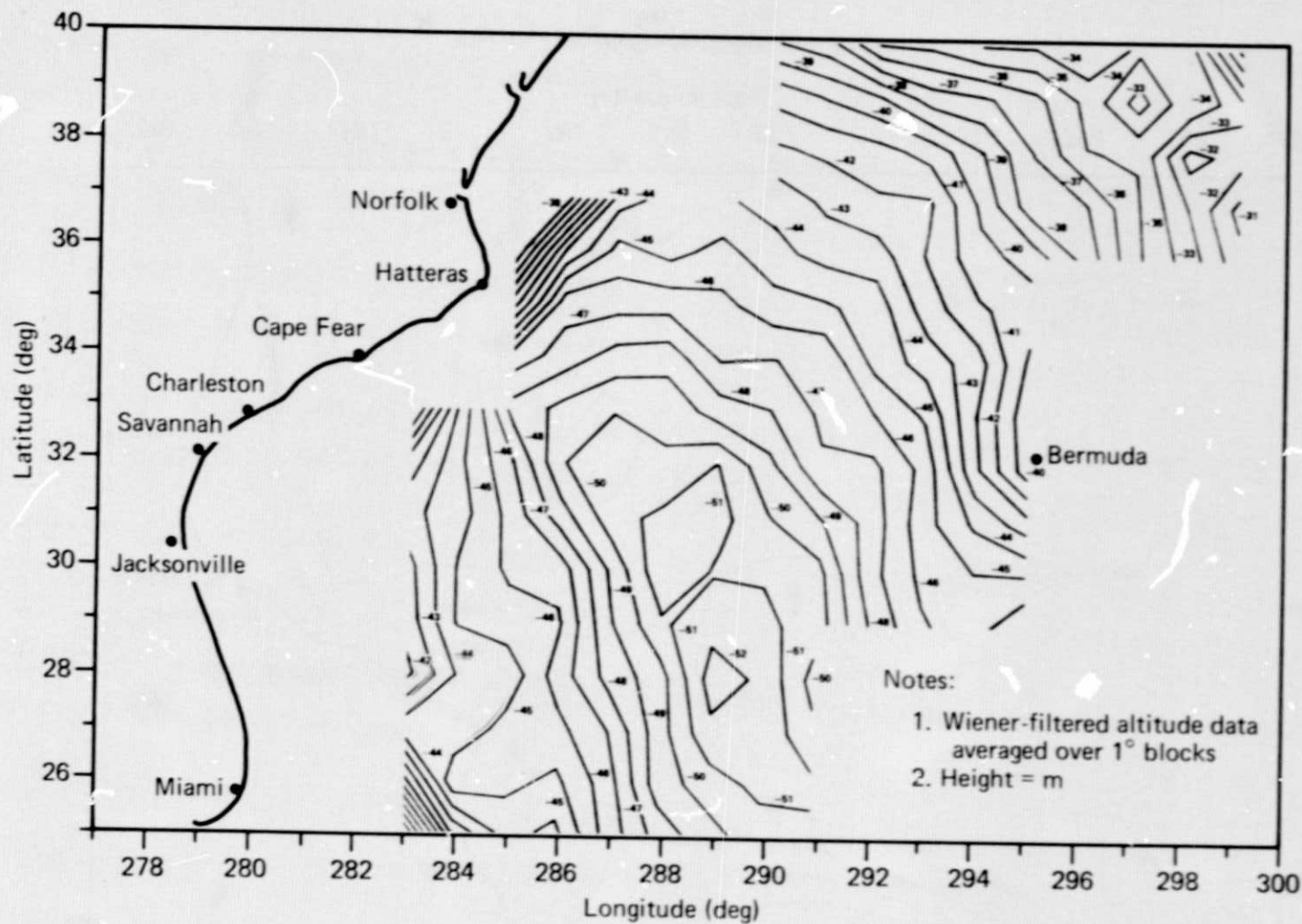


Fig. 9 Geoid Heights.

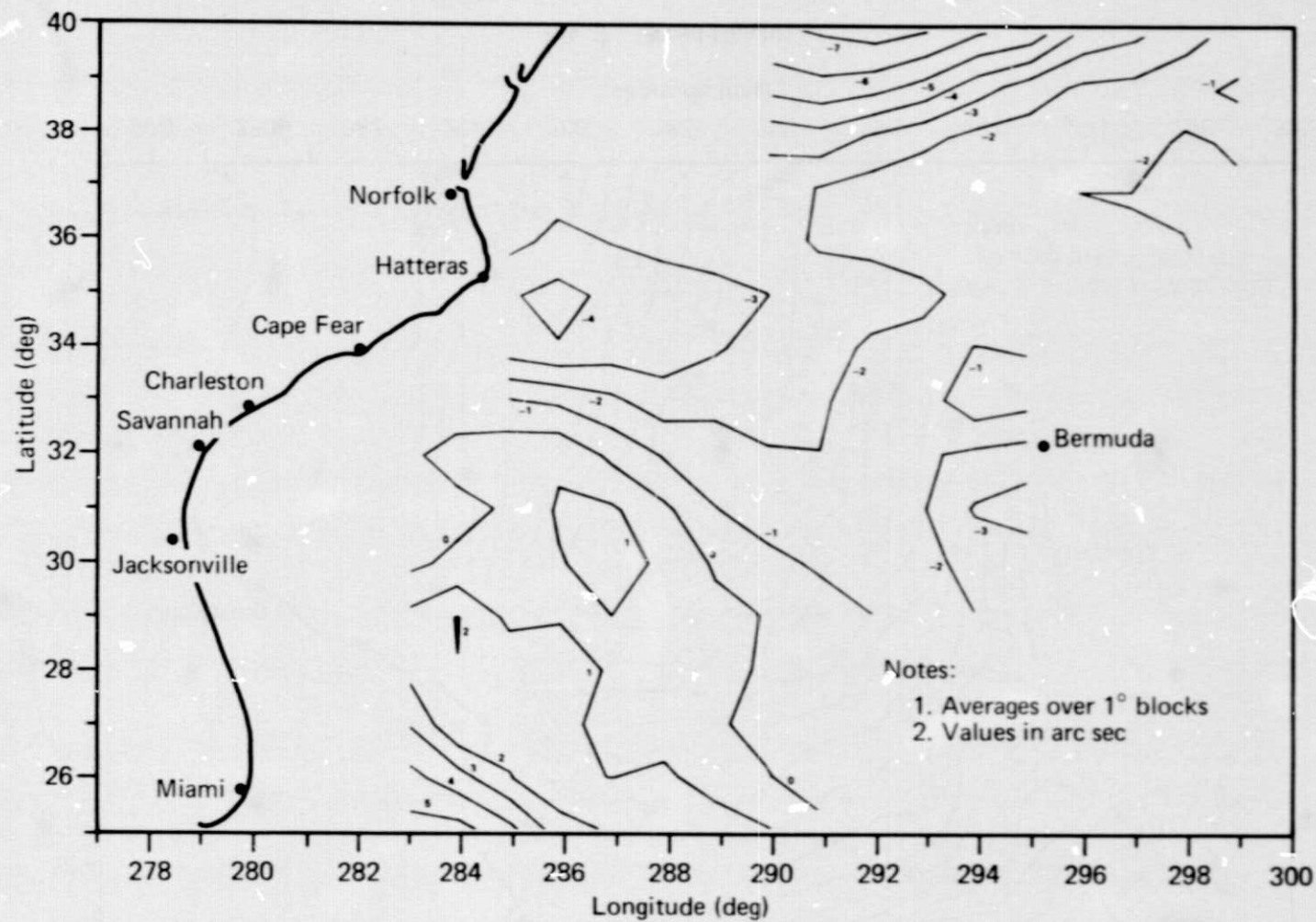


Fig. 10 North-South Deflection Angles.

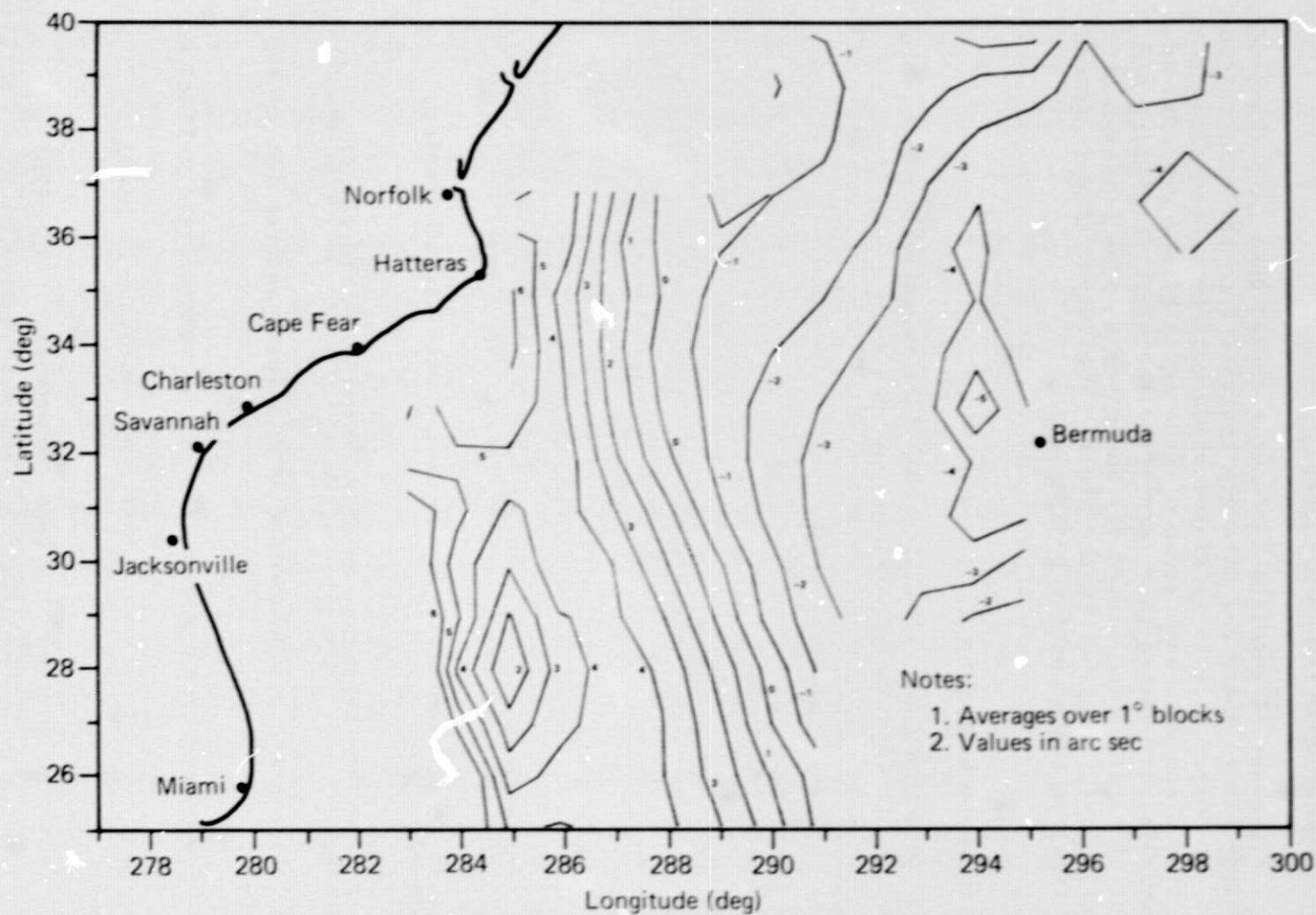


Fig. 11 East-West Deflection Angles.

4.2.1 Segmentation of Data Into Blocks

Processor II requires as input a sorted data file (latitude, longitude order) where all data are restricted to the calibration grid. An output file is generated where data have been segmented into grid areas with each group of data (grid block) preceded by a special header record that identifies the block (beginning and extent of latitude and longitude) and gives a count of the number of data points (records) in the block. The output file (segmented data file) is the input for Processor II.

4.2.2 Function Evaluation A

In each region, the filtered height measurements are represented as nth-order polynomials in φ and λ :

$$H_i = \sum_{\ell=0}^L \sum_{m=0}^{L-\ell} A_{\ell m}^{(i)} \Delta\varphi_i^{\ell} \Delta\lambda_i^m, \quad (1)$$

where

$$\Delta\varphi_i = \varphi - \varphi_i,$$

$$\Delta\lambda_i = \lambda - \lambda_i,$$

φ_i, λ_i = reference origin associated with the i th region,
and

$A_{\ell m}^{(i)}$ = fit parameters associated with the i th region.

The $A_{\ell m}$ parameters are determined from a least-squares fit to the filtered measurements.

Components of the deflection of the vertical are defined as

$$\xi = -\frac{1}{r} \frac{\partial H}{\partial \varphi} \quad (\text{n-s component}), \quad (2a)$$

$$\eta = -\frac{1}{r \cos \varphi} \frac{\partial H}{\partial \lambda} \quad (\text{e-w component}), \quad (2b)$$

Differentiating Eq. 1 yields

$$\xi = -\frac{1}{r} \sum_{\ell=0}^{L-1} \sum_{m=0}^{L-\ell-1} A_{\ell+1,m}^{(\ell+1)} \Delta \varphi^{\ell} \Delta \lambda^m, \quad (3a)$$

$$\eta = -\frac{1}{r \cos \varphi} \sum_{\ell=0}^{L-1} \sum_{m=0}^{L-\ell-1} A_{\ell,m+1}^{(m+1)} \Delta \varphi^{\ell} \Delta \lambda^m. \quad (3b)$$

Thus the fitted $A_{\ell m}$ values are also used to define the ξ and η components.

The results of this determination are presented in Figs. 12 through 14.

4.2.3 Function Evaluation B

This final method also uses the weighting function algorithm described in Refs. 5 and 6. However, here the $A_{\ell m}$ parameters are determined from a least-squares fit to the filtered along-track deflection angle measurements. In each region, the deflection angle is modeled as

$$\delta_i = -(\xi \cos A_z + \eta \sin A_z) \quad (4)$$

where A_z is the azimuth angle associated with the measurement point. ^zThe filtered along-track deflection angles are computed such that

$$\delta = \frac{\partial H}{\partial s} \quad (5)$$

where s defines distance along the satellite subtrack (thus, the need for the minus sign in Eq. 4). The functional forms for ξ and η are given by Eq. 3.

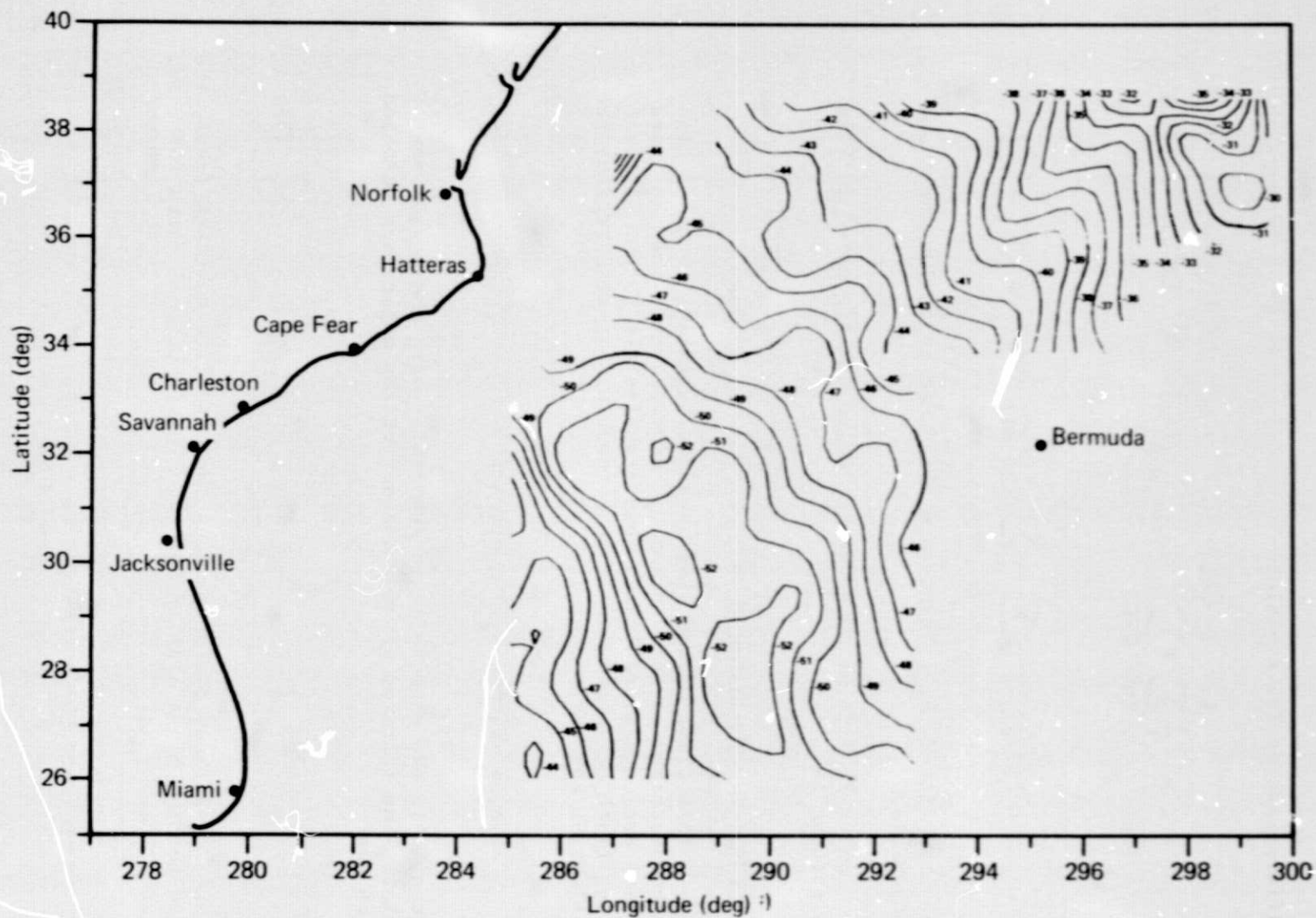


Fig. 12 Geoid Height Determined from GEOS-3 Altimeter Data
Determined from Filtered Along-Track Height Data.

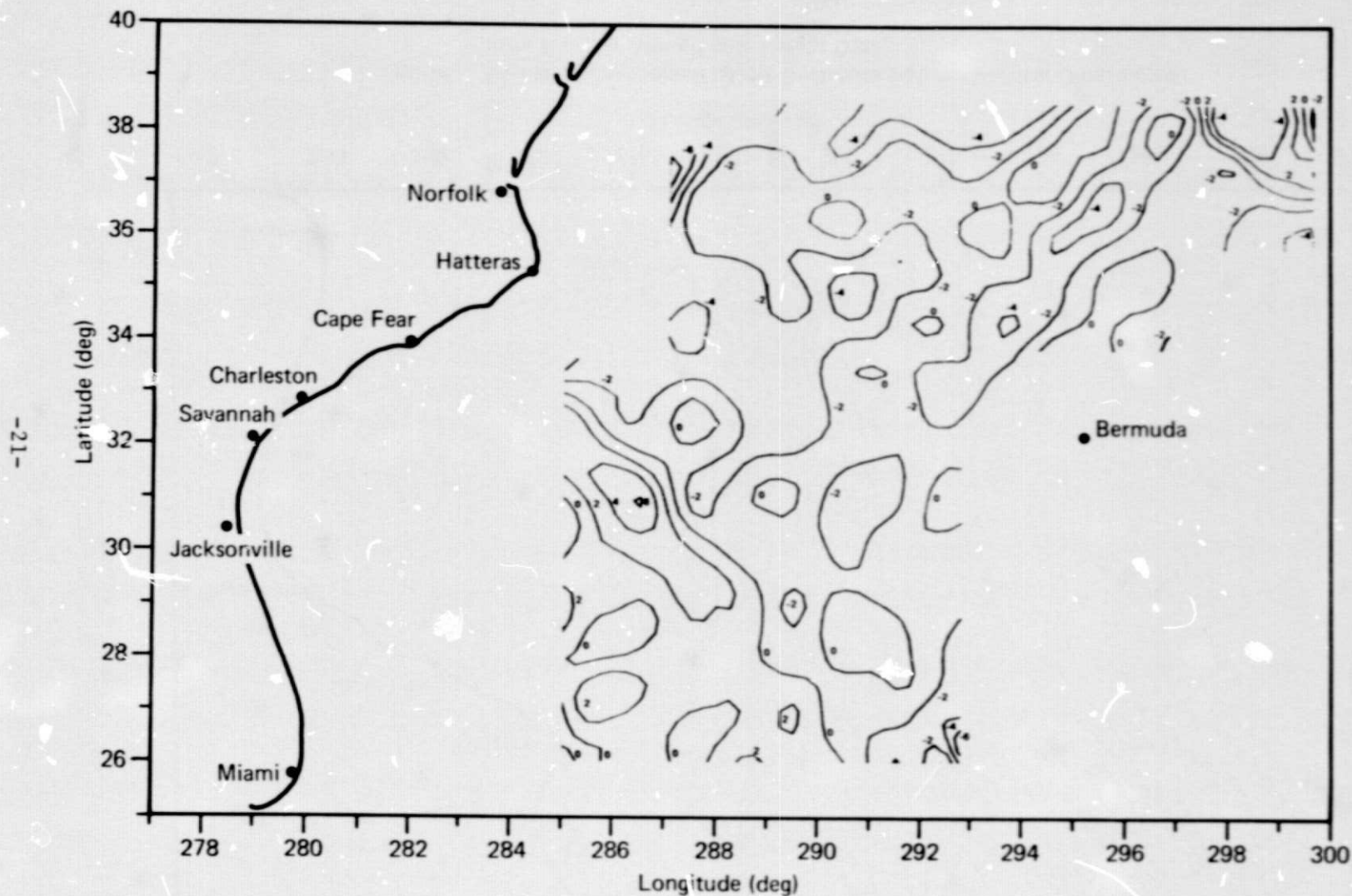


Fig. 13 North-South Component of the Deflections of the Vertical
Determined from Filtered Along-Track Height Data.

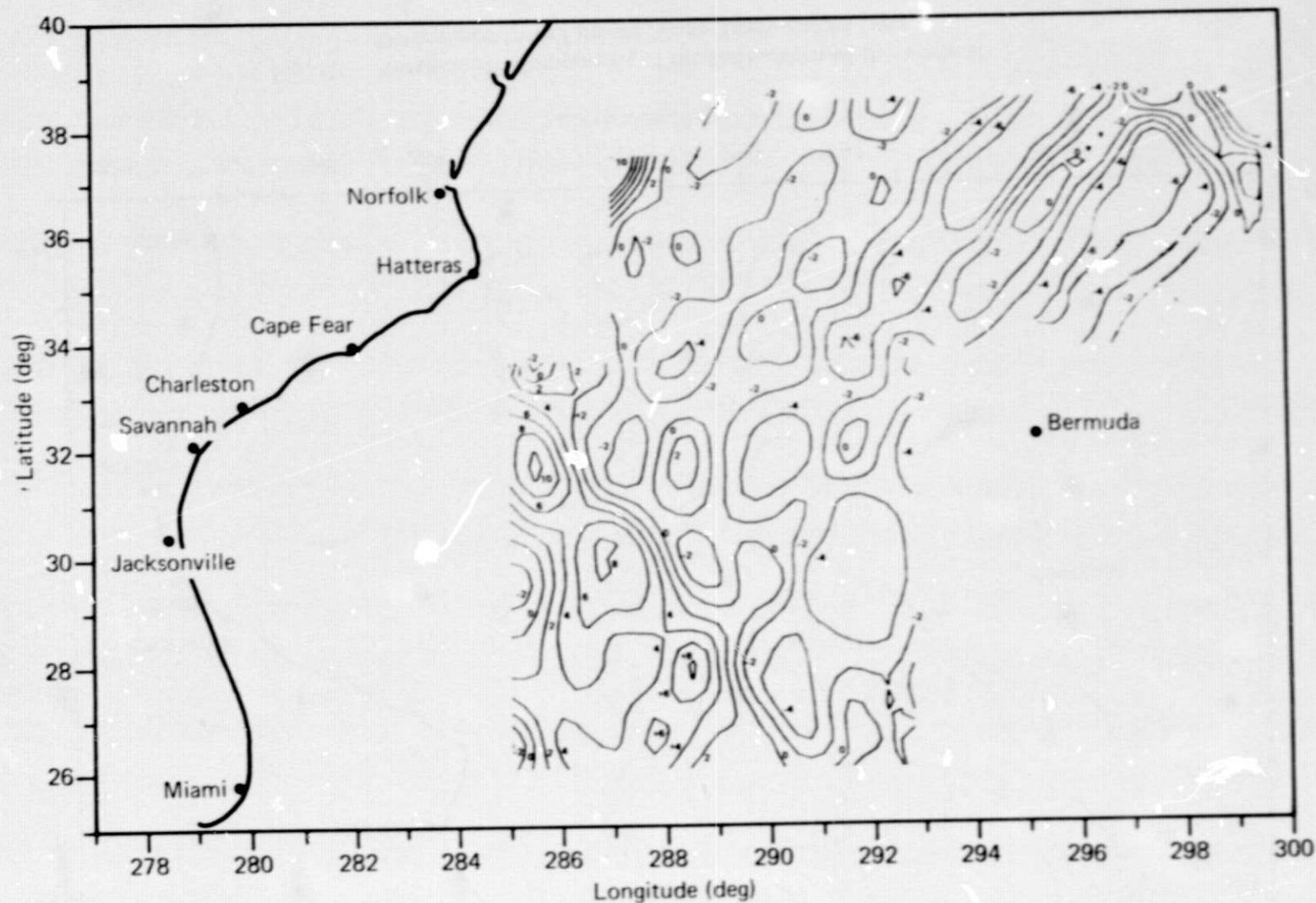


Fig. 14 East-West Component of the Deflections of the Vertical Determined from Filtered Along-Track Height Data.

In this least-squares fit, the A_{00} parameter is not estimated. Thus, the height as defined in Eq. 1 can only be computed minus the constant, A_{00} (i.e., $\Delta H_i = H^{(i)} - A_{00}$).

A value for $A_{00}^{(i)}$ is then estimated by computing the mean value of $H_m - \Delta H^{(i)}$ for the region being processed.

The results of this method are presented in Figs. 15 through 17.

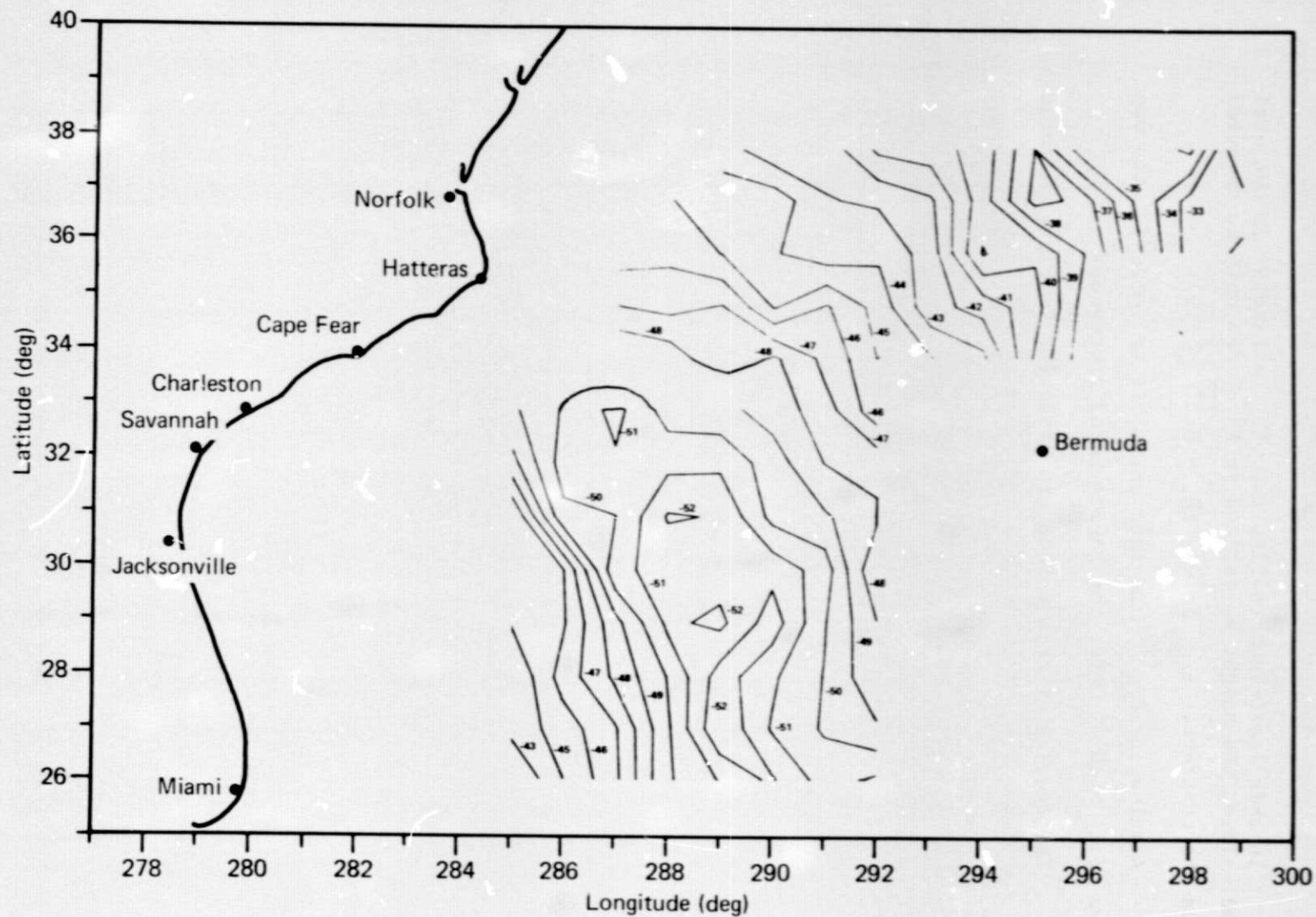


Fig. 15 Geoid Height Determined from GEOS-3 Altimeter Data Determined from Filtered Along-Track Deflection Data.

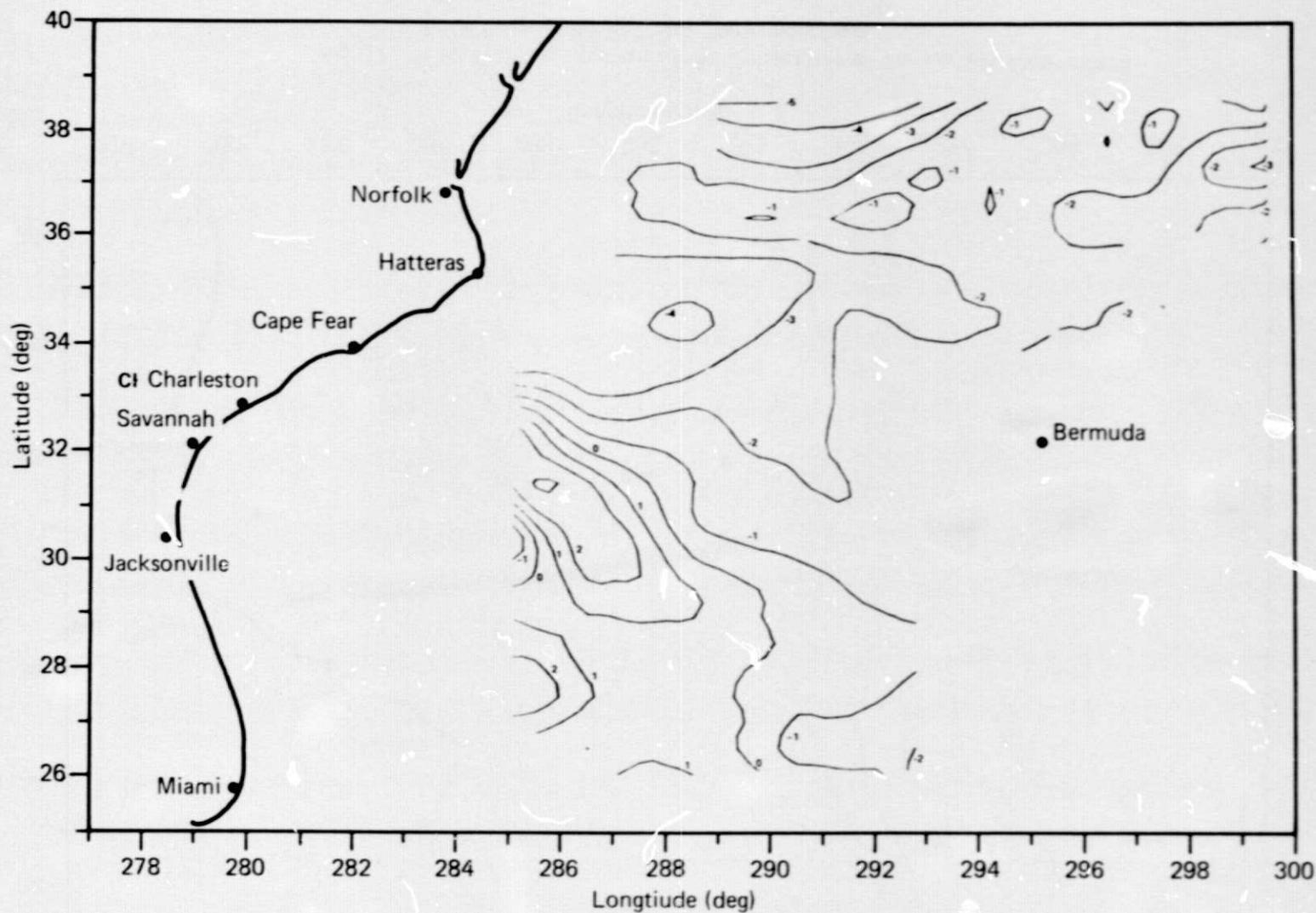


Fig. 16 North-South Component of the Deflections of the Vertical Determined from Filtered Along-Track Deflection Data.

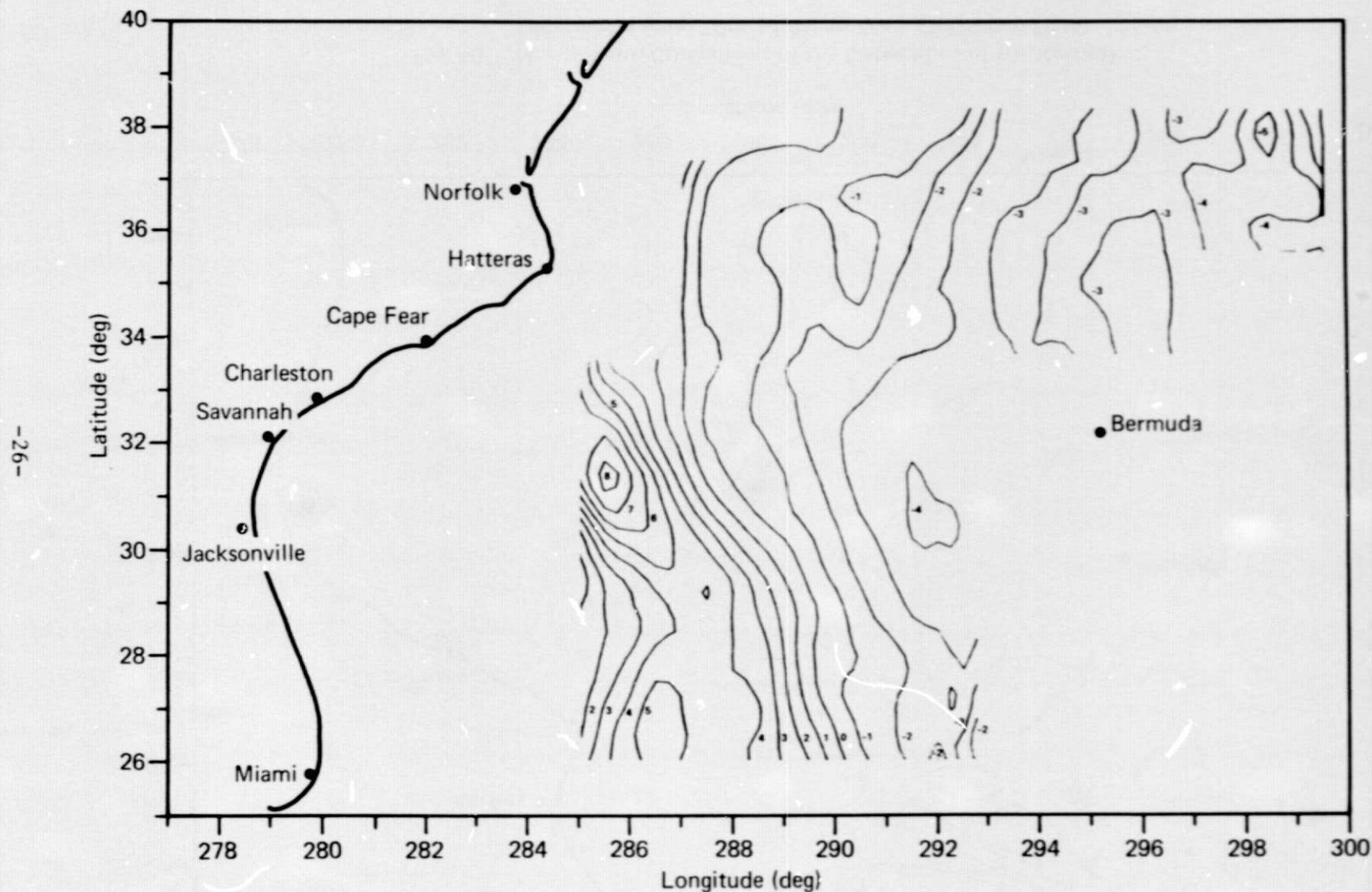


Fig. 17 East-West Component of the Deflections of the Vertical Determined from Filtered Along-Track Deflection Data.

5. CONCLUSIONS

The results obtained with the three different methods are very similar. The rms height difference among the three methods is only 0.5 m. The results also compare favorably with gravimetrically determined heights in the calibration area as well as with those obtained by Hadgigeorge and Trotter (Ref. 7). The rms of the deflection differences between the last two methods were 2 and 1.2 arc sec in ξ and η , respectively, versus 3 and 2.5 arc sec for the differences with method one.

In the final two methods, second-degree polynomials in φ and λ were used to model the height in each region. The rms of the fits to the filtered height and the along-track deflection data were 3.1 m and 3.2 arc sec, respectively, with both methods. The use of a higher degree polynomial in the fit did not significantly improve these results.

Ref. 7. G. Hadgigeorge and J. E. Trotter, "Short Arc Reductions of GEOS-3 Altimetric Data," Geophys. Res. Lett., Vol. 4, No. 6, Jun 1977.

ACKNOWLEDGMENTS

We would like to thank Robert E. Jenkins for generating the contour curves associated with the final results and Stanley C. Dillon for his assistance in the handling of the large volume of data that was processed. We are also indebted to Irene Hamil for undertaking the complicated task of typing and coordinating the original report and presentation material.

REFERENCES

1. "GEOS-C Mission Plan," TK-6340-01, Wallops Station, Wallops Island, VA, Aug 1974.
2. E. B. Anders, J. J. Johnson, A. D. Lasaine, P. W. Spikes, and J. T. Taylo, Digital Filters, NASA Report CR-130, December 1964.
3. A. Papoulis, Probability, Random Variables and Stochastic Processes, McGraw-Hill Book Co., New York, NY, 1965.
4. C. C. Tscherning and R. H. Rapp, "Closed Covariance Expressions for Gravity Anomalies, Geoid Undulations, and Deflections of the Vertical Implied by Anomaly Degree Covariance Models," Ohio State University Report No. 208, May 1974.
5. J. L. Junkins, G. W. Miller, and J. R. Jancaitis, "A Weighting Function Approach to Modeling of Irregular Surfaces," J. Geophys. Res., Vol. 78, No. 11, 10 Apr 1973.
6. J. R. Jancaitis and J. L. Junkins, "Modeling in n Dimensions Using a Weighting Function Approach," J. Geophys. Res., Vol. 79, No. 23, 10 Aug 1974.
7. G. Hadgigeorge and J. E. Trotter, "Short Arc Reductions of GEOS-3 Altimetric Data," Geophys. Res. Lett., Vol. 4, No. 6, Jun 1977.

1. Report No. NASA CR-141440		2. Government Accession No.		3. Recipient's Catalog No.	
4. Title and Subtitle GEOS-3 OCEAN GEOID INVESTIGATION				5. Report Date May 1978	
				6. Performing Organization Code	
7. Author(s) S. M. Yionoulis, A. Eisner, V.L. Pisacane, H. E. Black, L. L. Pryor				8. Performing Organization Report No.	
				10. Work Unit No.	
9. Performing Organization Name and Address The Johns Hopkins University Applied Physics Laboratory Johns Hopkins Road Laurel, MD 20810				11. Contract or Grant No. P57,606(G)	
				13. Type of Report and Period Covered Final Report	
12. Sponsoring Agency Name and Address National Aeronautics and Space Administration Wallops Flight Center Wallops Island, VA 23337				14. Sponsoring Agency Code	
15. Supplementary Notes					
16. Abstract A determination of the fine-scale sea surface topography in the GEOS-3 calibration area using the radar altimeter data is presented. Estimates of the north-south and east-west components of the deflections of the vertical as well as values of the geoidal heights are made. Three major stages of processing are used in obtaining the final results. The first two use pass processors; in the final stage, the processor combines all the pass results to compute the final results. The results obtained compare favorably with gravimetrically determined geoids for this calibration area.					
17. Key Words (Suggested by Author(s)) GEOS-3, geoid, altimetry, deflection of vertical			18. Distribution Statement Unclassified - unlimited STAR Category - 42,46,48		
19. Security Classif. (of this report) Unclassified		20. Security Classif. (of this page) Unclassified		21. No. of Pages 33	
				22. Price*	